Selective Detection of Dynamics-Complete Set of Correlations via Quantum Channels

Ze Wu,[1,2,*] Ping Wang,[3,4,*] Tianyun Wang,[1,2] Yuchen Li,[1,2] Ran Liu,[1,2] Yuquan Chen,[1,2] Xinhua Peng,[1,2,5,†] and Ren-Bao Liu[4,6,7,8,‡]

[1]*CAS Key Laboratory of Microscale Magnetic Resonance and School of Physical Sciences, University of Science and Technology of China, Hefei 230026, China*

[2]*CAS Center for Excellence in Quantum Information and Quantum Physics, University of Science and Technology of China, Hefei 230026, China*

[3]*Faculty of Arts and Sciences, Beijing Normal University, Zhuhai 519087, China*

[4]*Department of Physics, The Chinese University of Hong Kong, Shatin, New Territories, Hong Kong, China*

[5]*Hefei National Laboratory, University of Science and Technology of China, Hefei 230088, China*

[6]*Centre for Quantum Coherence, The Chinese University of Hong Kong, Shatin, New Territories, Hong Kong, China*

[7]*The Hong Kong Institute of Quantum Information Science and Technology, The Chinese University of Hong Kong, Shatin, New Territories, Hong Kong, China*

[8]*New Cornerstone Science Laboratory, The Chinese University of Hong Kong, Shatin, New Territories, Hong Kong, China*

(Received 27 November 2023; revised 25 February 2024; accepted 1 April 2024; published 16 May 2024)

Correlations of fluctuations are essential to understanding many-body systems and key information for advancing quantum technologies. To fully describe the dynamics of a physical system, all time-ordered correlations (TOCs), i.e., the dynamics-complete set of correlations are needed. The current measurement techniques can only access a limited set of TOCs, and there has been no systematic and feasible solution for extracting the dynamic-complete set of correlations hitherto. Here we propose a platform-universal protocol to selectively detect arbitrary types of TOCs via quantum channels. In our method, the quantum channels are synthesized with various controls, and engineer the evolution of a sensor-target system along a specific path that corresponds to a desired correlation. Using nuclear magnetic resonance, we experimentally demonstrate this protocol by detecting a specific type of fourth-order TOC that has never been accessed previously. We also show that the knowledge of the TOCs can be used to significantly improve the precision of quantum optimal control. Our method provides a new toolbox for characterizing the quantum many-body states and quantum noise, and hence for advancing the fields of quantum sensing and quantum computing.

DOI: 10.1103/PhysRevLett.132.200802

Introduction.—Quantum metrology and sensing uses quantum resources (coherence, squeezing, entanglement, etc.) to enhance the acquisition of information from target systems [1–3]. Numerous works have demonstrated the advantages of quantum metrology and sensing in detection, imaging, and spectroscopy [4–7]. A legitimate question is: Can quantum metrology and sensing achieve tasks that are beyond the practical capability of their classical counterparts? We believe the answer is positive. There are already stimulating examples, such as the exponential saving of the number of measurement shots for phase estimation using quantum algorithm [8], the exponential saving of experimental time in distinguishing different types of quantum evolutions using quantum instruments [9], and the realization of physical parameters in the complex plane using evolution of a quantum sensor [10,11]. In this paper, we experimentally demonstrate that quantum sensing can exponentially extend the scope of accessible correlation functions in a target system.

Information about a system is essentially the set of correlations among the observables (say, $B_1, B_2, \cdots$) at different locations and times [12–14]. In quantum mechanics, different observables in general do not commute (e.g., $\hat{B}_1\hat{B}_2 \neq \hat{B}_2\hat{B}_1$), and different orderings of the observables correspond to different correlations. A set of N observables in quantum mechanics would have $N!$ differently ordered correlations. For observables at times (e.g., $\hat{B}_1, \hat{B}_2, \hat{B}_3, \cdots$ at times $t_1 < t_2 < t_3 < \cdots$), the time-ordered correlations (TOCs) are particularly important, since the quantum evolution, captured by a time-dependent density matrix $\hat{\rho}(t)$, can be fully constructed by correlations like $\langle \hat{B}_a\hat{B}_b\cdots\hat{B}_d\hat{B}_l\cdots\hat{B}_j\hat{B}_i\rangle = \mathrm{Tr}_\mathrm{B}[\hat{B}_l\cdots\hat{B}_j\hat{B}_i\hat{\rho}(0)\hat{B}_a\hat{B}_b\cdots\hat{B}_d]$, in which the observables are ordered on a contour time (with time-ordering $t_l > \cdots > t_j > t_i$ and counter-time-ordering $t_a < t_b < \cdots < t_d$). The Nth or correlations contain 2^{N-1} TOCs and $N! - 2^{N-1}$ out-of-time-order correlations (OTOCs). While the OTOCs are of their own

interest, the TOCs are dynamics complete. The knowledge of TOCs in an environment is critical to understanding the dynamics of an open quantum system and to optimizing its quantum control, which is relevant to quantum information technology [15–17].

However, the selective extraction of different types of TOCs is still elusive. The existing techniques such as noise spectroscopy and nonlinear spectroscopy can only extract some special types of TOCs [18–21]. In classical noise spectroscopy [19,21], the correlations like $\langle B_1 B_2 \cdots B_N \rangle$ are obtained by measuring the observables at different times. For quantum observables, such noise correlations should be replaced with the expectation values of symmetrically ordered observables, such as $\frac{1}{2}\langle\{\hat{B}_1, \hat{B}_2\}\rangle$ and $\frac{1}{4}\langle\{\{\hat{B}_1, \hat{B}_2\}, \hat{B}_3\}\rangle$, where the anticommutator $\{\hat{A}, \hat{B}\} = \hat{A}\hat{B} + \hat{B}\hat{A}$ reduces to the usual product for classical quantities. On the other hand, in classical nonlinear spectroscopy [18,20], under the perturbation by a weak classical force, the response of a target quantum system to a certain (say, the third) order of the force corresponds to correlations like $i^3\langle\{\hat{B}_3, [\hat{B}_2, [\hat{B}_1, \hat{B}_0]]\}\rangle$, in which the commutators $[\hat{A}, \hat{B}] = \hat{A}\hat{B} - \hat{B}\hat{A}$ result from the quantum evolution of the target system under the classical force. These conventional techniques can extract only two types of TOCs, leaving exponentially more correlations ($2^{N-1} - 2$ types in the Nth order) inaccessible.

A recent proposal of quantum nonlinear spectroscopy has the potential to selectively detect all types and orders of TOCs [22]. However, the experimental implementation of this scheme is challenging for two main reasons. First, multiple shots of quantum measurement with high fidelity and high speed are required. Second, the scheme applies only to single quantum sensors since in many (say, K) independent sensors, the correlations of N shots of measurement would scale as $1/K^{N-1}$, which vanishes for large K and $N > 1$. A previous experiment on quantum nonlinear spectroscopy uses three shots of measurement to detect the fourth-order correlations but still cannot separate different types of TOCs [23].

In this Letter, we present a novel protocol for selectively extracting a dynamics-complete set of TOCs by utilizing quantum channels that are synthesized through controllable physical processes. Compared to previous techniques [18–23], this protocol is applicable for a wide range of quantum systems. As an example, we experimentally demonstrate the selective extraction of a specific fourth-order TOC, C^{+--+}, that has never been measured before. Further, we numerically demonstrate that this type of TOC can be utilized to optimize the quantum logic gates within a strongly coupled quantum environment, leading to a significant enhancement in the final state fidelity. It should be mentioned that the previous experiments measuring the second-order TOCs [18,24] can be understood as the lower-order prototypes of our general scheme.

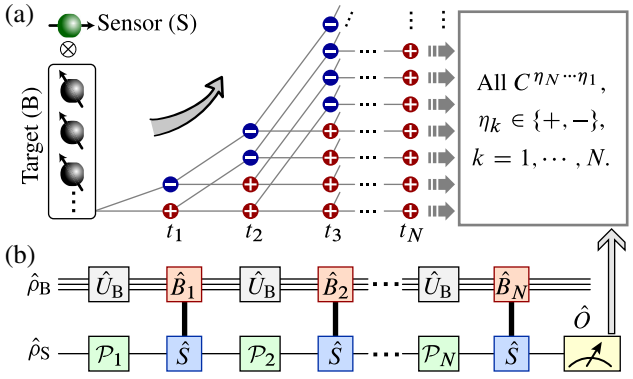

FIG. 1. Protocol for extracting time-ordered correlations. (a) Time-ordered correlations of the quantum many-body target. The evolution of the system gives rise to a variety of TOCs, whose number exponentially grows with the orders. (b) General quantum circuit to measure arbitrary Nth order TOCs. The sensor and target are initially at $\hat{\rho}_S$ and $\hat{\rho}_B$, respectively. N quantum channels $\mathcal{P}_i$ $(i = 1, 2, \ldots, N)$ are interleaved before N brief interaction processes. $\hat{U}_B$ is the free evolution of the target. Finally, the observable $\hat{O}$ is measured on the sensor.

General theory.—Consider a quantum sensor (S) that interacts with a quantum target (B) via

$$\hat{V}(t) = \hat{S} \otimes \hat{B}(t). \tag{1}$$

The protocol depicted in Fig. 1 is used to measure arbitrary Nth-order TOCs. Firstly, the quantum sensor is prepared to an initial state $\hat{\rho}_S$. Then the coupled sensor-target system undergoes N interaction processes (each with a duration of δt) at times $t_1, t_2, \ldots, t_N$, respectively. Between the $(i-1)$-th and the ith interaction processes, the quantum channel $\mathcal{P}_i$ is applied to the sensor, and the target, decoupled from the sensor, is undergoing free evolution. The quantum channels $\mathcal{P}_i$ are constructed through the linear superposition of controllable physical processes, such as spin rotations of different directions [25–27]. Finally, the observable $\hat{O}$ is measured on the quantum sensor.

Theoretically, the measured signal can be formulated in superoperator form [28]

$$S_N = \mathrm{Tr}\left[\hat{O}\mathcal{T}\prod_{i=1}^{N}(\mathcal{U}_I^{(i)}\mathcal{P}_i)(\hat{\rho}_S \otimes \hat{\rho}_B)\right]. \tag{2}$$

Here $\mathcal{U}_I^{(i)}\hat{\rho} = \mathcal{T}\exp\{-i\int_{t_i}^{t_i+\delta t}[\hat{V}(t_i), \hat{\rho}]dt\}$ describes the evolution of the sensor-target system in the duration of t_i to $t_i + \delta t$, and $\mathcal{T}$ is the time-ordering operator. We can expand $\mathcal{U}_I^{(i)}$ to its first order of δt [22]:

$$\mathcal{U}_I^{(i)} \approx \mathcal{S}^0\mathcal{B}^0(t_i) + 2\delta t[\mathcal{S}^- \otimes \mathcal{B}^+(t_i) + \mathcal{S}^+ \otimes \mathcal{B}^-(t_i)], \tag{3}$$

where the superoperators $\mathcal{B}^{\pm}(t)$ are defined as $\mathcal{B}^{-}\hat{\rho} \equiv [\hat{B},\hat{\rho}]/(2i)$ (commutator) and $\mathcal{B}^{+}\hat{\rho} \equiv \{\hat{B},\hat{\rho}\}/2$ (anticommutator). For convenience, we also set $\mathcal{S}^0 = \mathcal{B}^0(t_i) = \mathbb{1}$. Therefore, S_N can be calculated up to the order of δt^N, which is the linear sum of different types of TOCs ($C^{\eta_N\cdots\eta_1}$):

$$S_N = \sum_{\eta_i\in\{\pm,0\}} \delta t^{\Theta} A^{\bar{\eta}_N\cdots\bar{\eta}_1} C^{\eta_N\cdots\eta_1} + O(\delta t^{N+1}). \tag{4}$$

Here $\bar{\eta}_i = -\eta_i$, and $\Theta = \sum_{i=1}^{N} |\eta_i|$ ($\eta_i \in \{0,+,-\}$) is the order of each term. If $\eta_{1,2,\ldots,N} \neq 0$, then $C^{\eta_N\cdots\eta_1} = \mathrm{Tr}_{\mathrm{B}}[\mathcal{B}^{\eta_N}(t_N)\cdots\mathcal{B}^{\eta_1}(t_1)\hat{\rho}_{\mathrm{B}}]$ is the Nth order TOCs. While if there are k instances of $\eta_i = 0$, it reduces to TOCs with order $N-k$. Since $\mathcal{S}^{\pm}$ are always adjoint with $\mathcal{B}^{\mp}(t_i)$ in Eq. (3), the coefficient multiplied with $C^{\eta_N\cdots\eta_1}$ in Eq. (4) is always $A^{\bar{\eta}_N\cdots\bar{\eta}_1}$, which reads as

$$A^{\bar{\eta}_N\cdots\bar{\eta}_1} = \mathrm{Tr}_{\mathrm{S}}\left[\hat{O}\mathcal{T}\prod_{i=1}^{N}(\mathcal{S}^{\bar{\eta}_i}\mathcal{P}_i)\hat{\rho}_{\mathrm{S}}\right]. \tag{5}$$

In order to measure the Nth order TOC $C^{\gamma_N\cdots\gamma_1}$, a set of quantum channels $\{\mathcal{P}_1,\mathcal{P}_2,\ldots,\mathcal{P}_N\}$ is designed to ensure $A^{\bar{\eta}_N\cdots\bar{\eta}_1} = 0$, unless $\eta_N\cdots\eta_1 = \gamma_N\cdots\gamma_1$. Consequently, only one term in Eq. (4) is retained, and the signals of the desired correlation are selectively extracted.

Experimental demonstration.—As an example, we experimentally demonstrate the measurement of a specific fourth-order TOC, C^{+--+}, which has never been obtained by conventional methods. Consider a spin-1/2 quantum sensor that interacts with the quantum target via $\hat{V}(t) = \hat{S}_z \otimes \hat{B}(t)$. The quantum sensor is initially prepared at $\hat{\rho}_{\mathrm{S}} = (\mathbb{1} + p\hat{\sigma}_z)/2$ (p denotes the polarization of the sensor). To measure C^{+--+} of $\hat{B}(t)$, we choose the observable $\hat{O} = \hat{\sigma}_y$, and design four quantum channels as follows [28]:

$$\begin{aligned}\mathcal{P}_{1,4} &= [\mathcal{R}_y(\pi/2) - \mathcal{R}_y(-\pi/2)]/2,\\ \mathcal{P}_2 &= [\mathcal{R}_x(\pi/2) - \mathcal{R}_x(-\pi/2)]/2,\\ \mathcal{P}_3 &= [\mathcal{R}_x(\pi/2) + \mathcal{R}_x(-\pi/2)]/2.\end{aligned} \tag{6}$$

Here $\mathcal{R}_\alpha(\theta)$ is the spin rotation around the α axis by the θ angle. The scheme can be illustrated by the channel diagram depicted in Fig. 2(a). In the Liouville space spanned by complete Pauli basis $\{\mathbb{1},\hat{\sigma}_x,\hat{\sigma}_y,\hat{\sigma}_z\}$, the initial state $\hat{\rho}_{\mathrm{S}}$ and observable $\hat{O}$ can be represented by four-dimensional vectors, and the superoperators like $\mathcal{S}^{\pm}$ and $\mathcal{P}_i$ are represented by 4×4 matrices. For example, the construction of $\mathcal{P}_1$ is shown in Fig. 2(b). Thus in Fig. 2(a), the nonvanishing coefficient A^{-++-} that is associated with C^{+--+} corresponds to a connected path (in solid line) that starts from the $\hat{\sigma}_z$ component of the initial state $\hat{\rho}_{\mathrm{S}}$ and ends at the final observable $\hat{\sigma}_y$. The coefficients associated with other paths vanish. Since $A^{-++-} = p$, the final measurement signal $S_4 \equiv \langle\hat{\sigma}_y\rangle$ in Eq. (2) is given by [28]

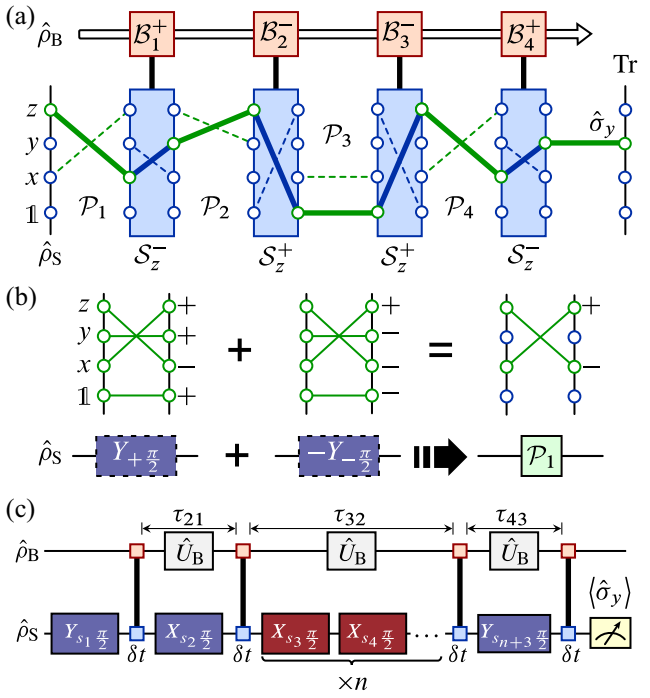

FIG. 2. Experimental scheme for measuring C^{+--+}. (a) Quantum channel diagram for measuring the fourth-order TOC C^{+--+}. The thick line represents the connected path that survives through the interactions and the quantum channels defined in Eq. (6) which isolates the signal C^{+--+}. (b) An example of quantum channel constructed by spin rotations $Y_{+\pi/2}$ and $Y_{-\pi/2}$. The green lines illustrate the matrix elements of the superoperators in the representation of Pauli basis. (c) Factorization of the measurement sequence into superposition of the unitary sequences. The label index s_i ($i = 1,\ldots,n+3$) can take two values $+1$ or -1; thus there are totally 2^{n+3} unitary sequences. The operations in the red box make the sequence robust against $\pi/2$ rotation error.

$$S_4 = \delta t^4 p C^{+--+} + O(\delta t^6). \tag{7}$$

As a result, C^{+--+} can be measured via $C^{+--+} \approx S_4/(p\delta t^4)$.

The scheme proposed above is experimentally demonstrated by using nuclear spins at room temperature on a Bruker Avance III 400 MHz nuclear magnetic resonance spectrometer. The sample is carbon-13 labeled acetic acid ($^{13}CH_3COOH$) dissolved in heavy water (D_2O). The ^{13}C nucleus serves as the central spin sensor, while three ^{1}H nuclei in the methyl group ($-^{13}CH_3$) comprise the quantum target to be detected. In doubly rotating the frame of ^{13}C and ^{1}H nuclei, the interaction between the sensor and target is $\hat{V} = J\hat{S}_z^{\mathrm{C}} \otimes \sum_{i=1}^{3}\hat{I}_{i,z}^{\mathrm{H}}$ ($J = 2\pi\times 129.6$ rad/s). The free evolution of the target is realized by applying a radio frequency (RF) field along the x axis on ^{1}H spins. During the period of free evolution, the interaction between the sensor and the target is negligible, as compared to the Hamiltonian of the target $\hat{H}_{\mathrm{B}} = \Omega\sum_{i=1}^{3}\hat{I}_{i,x}^{\mathrm{H}}$

($\Omega \approx 2\pi \times 24000$ rad/s). As a result, in the interaction picture of $\hat{H}_B$, the total Hamiltonian takes the form of Eq. (1), where $\hat{B}(t) = J\sum_{i=1}^{3} \hat{I}_{i,z}^{H}(t)$ and $\hat{I}_{i,z}^{H}(t) = e^{i\hat{H}_B t}\hat{I}_{i,z}^{H}e^{-i\hat{H}_B t}$. Figure 2(c) depicts the experimental quantum channel sequence used to measure the fourth-order TOC, C^{+--+}. Initially, the sensor is polarized to the thermal equilibrium state $\hat{\rho}_S = (\mathbb{1} + 2p_C\hat{S}_z^C)/2$ with $p_C \approx 8.0 \times 10^{-5}$, which creates the z polarized state. Next, the quantum channels in Eq. (8) are implemented by superimposing the measurement signals with rotation pulses $\mathcal{R}_\alpha(\pm\pi/2)$ along various rotating axes α. The signals are acquired by measuring the expectation value $\langle\hat{\sigma}_y^C\rangle$ on the sensor spin.

To deal with the nonideality of experimental parameters, we design an error-robust quantum channel. In experiments, the error of $\pi/2$ rotation pulse ($\delta\phi$, relatively 2%–3%) will introduce an error of order $\delta\phi$ to the $\mathcal{P}_3$ channel, which mixes the lower-order TOCs into the fourth-order signals C^{+--+} [28]. In order to address this issue, we iterate the $\mathcal{P}_3$ channel for n times, yielding $(\mathcal{P}_3)^n = [\mathcal{R}_x(\pi/2 + \delta\phi) + \mathcal{R}_x(-\pi/2 - \delta\phi)]^n/2^n$. This enables us to achieve a quantum channel that exponentially converges toward the ideal $\mathcal{P}_3$ channel [28]. Therefore, the final signal S_4 can be constructed as a weighted sum of the measured signals ($\langle\hat{\sigma}_y^C\rangle$) obtained from the 2^{n+3} unitary processes,

$$S_4 = \frac{1}{2^{n+3}} \sum_{\{s_1,\ldots,s_{n+3}\}} s_1 s_2 s_{n+3} S_{s_1,\ldots,s_{n+3}}. \quad (8)$$

Here $s_i = \pm 1$, and $S_{s_1,\ldots,s_{n+3}}$ represents the signal associated with the indices $\{s_1,\ldots,s_{n+3}\}$ that control the rotation angle.

Figure 3(a) shows the measured fourth signal S_4 versus the evolution time $\tau_{21} = t_2 - t_1$ for $\delta t = 0.5$ ms, with blue and black scatters representing the cases of $n = 1$ and $n = 3$, respectively. Here, $\tau_{32} = t_3 - t_2$ and $\tau_{43} = t_4 - t_3$ are fixed at 10 μs. To obtain the absolute value $\langle\hat{\sigma}_y^C\rangle$ of a single ^{13}C, the signal has been normalized with respect to the free induction decay signal of the ^{13}C nuclear spin in the equilibrium state. For comparison, we present the ideal signal in Fig. 3(a) in the green dashed line, and it is expressed as follows [28]:

$$S_4^{\text{ideal}} = \frac{N_H}{16}\delta t^4 J^4 \sin(\omega\tau_{21})\sin(\omega\tau_{43}) + O(\delta t^6). \quad (9)$$

Here N_H is the number of protons. The measured signal (S_4) for $n = 1$ (blue scatters) exhibits a significant deviation (with a relative error of 112.2%) from the ideal result. In contrast, the measured signal for $n = 3$ (black scatters) exhibits better convergence (with a relative error of 23.5%) to the ideal signal (green dashed line). This demonstrates the robustness of our protocol against the pulse error. Another notable source of error is the decoherence caused by RF inhomogeneity, which leads to a reduction of signal amplitude and degradation of spectral resolution [28,31].

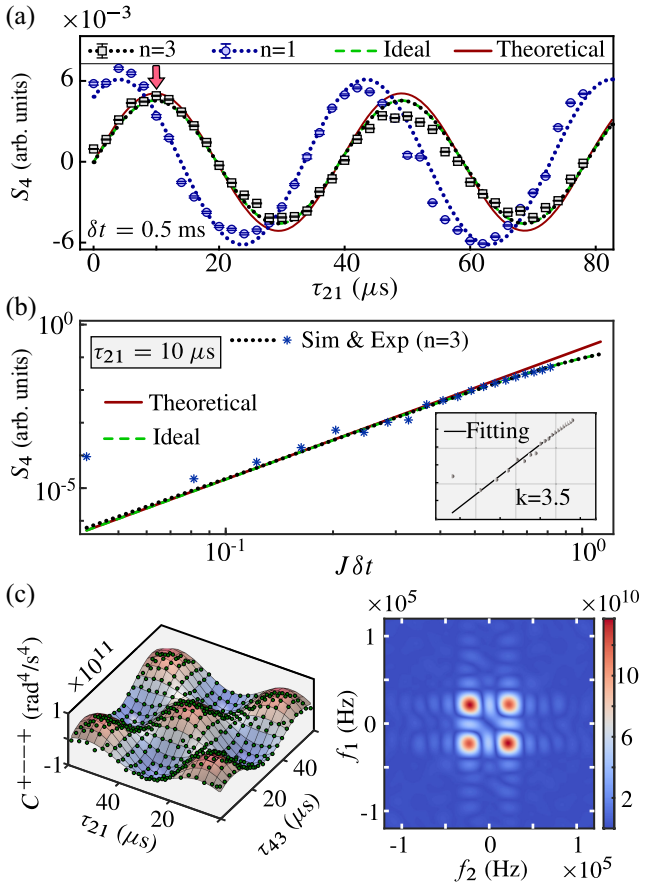

FIG. 3. Experimental results. (a) Measured signal of S_4 versus τ_{21} for $n = 1$ (blue scatters) and $n = 3$ (black scatters) when $\delta t = 0.5$ ms and $\tau_{32} = \tau_{43} = 10$ μs. The green dashed line denotes the ideal signal with high-order contributions [see Eq. (9)]. The red line denotes the theoretical signal of C^{+--+}. (b) Logarithm plot of the measured amplitude of S_4 versus $J\delta t$, which is obtained by the measured signal at $\tau_{21} = \tau_{32} = \tau_{43} = 10$ μs. (c) Green dots in the left figure represent the measured C^{+--+} as a function of evolution time τ_{21}, τ_{43}, with τ_{32} fixed. The mesh surface corresponds to the theoretical values. The 2D spectral structure of C^{+--+} with respect to τ_{21} and τ_{43} is shown in the right figure.

To demonstrate that the signal obtained by the scheme in Fig. 3(a) is dominated by fourth-order TOCs, we plot the amplitude of S_4 as a function of $J\delta t$ in Fig. 3(b). The amplitude is measured by the maximum value of S_4 at a fixed evolution time, $\tau_{21} = \tau_{32} = \tau_{43} = 10$ μs [indicated by the red arrow in Fig. 3(a)]. As shown in the inset of Fig. 3(b), the linear fitting yields a slope of $k = 3.5$, which is close to the ideal power exponent $k = 4$ given by Eq. (9). This indicates that the measured S_4 is dominated by the fourth-order correlations and can therefore be used to reconstruct C^{+--+}. The slight deviation from the ideal exponent ($k = 4$) results from the higher-order contributions ($\sim\delta t^{>4}$) of the dynamics due to relative long δt.

The selection of optimized δt is a trade-off in experiment, as shown in the Supplemental Material [28]. We then measure S_4 as a function of τ_{21} and τ_{43} (note that C^{+--+} does not depend on τ_{32}), and reconstruct C^{+--+} by using Eq. (7). The 2D data of C^{+--+} are shown in the left graph of Fig. 3(c) (green dots), which is consistent with the theoretical results (mesh surface). The Fourier transform of the 2D data is shown in the right graph of Fig. 3(c), which is the spectral feature of C^{+--+}.

Application.—Owing to the fact that TOCs completely characterize the dynamical disturbance caused by the quantum bath, one of the significant applications of this method is the high-precision quantum optimal control. We show that the TOC C^{+--+} measured here can be used to extraordinarily promote the quantum optimal control. For example, let us consider the previous model but with the quantum bath at infinitely high temperature (i.e., $\rho_B = \mathbb{1}/2^N$). The nonzero TOCs up to fourth order are C^{++}, C^{++++}, and C^{+--+}, as shown in the Supplemental Material [28]. Since the commutation in C^{+--+} always vanishes for a classical stochastic field, the presence of nonzero C^{+--+} then indicates that the bath is a quantum environment which cannot be described by semiclassical theory [24,31]. We here numerically demonstrate that the knowledge about C^{+--+} detected in this paper can promote the precision of Hadamard gate and Pauli-X gate.

As illustrated in Fig. 4, the fidelity ($F = \sqrt{\langle\psi|\rho_f|\psi\rangle}$) between the actual final state ρ_f and the ideal state $|\psi\rangle$ is approximately 90% when the quantum gates are not optimized. After optimized based on the second-order master equation with TOC C^{++} (which is equivalent to the Redfield master equation), the final state fidelity converges to 99.99% (see red triangles in Fig. 4). In order to achieve further breakthroughs in fidelity, the higher-order TOCs become indispensable. Based on the TOC C^{++++}, the fidelity F is optimized to 99.999% (the green squares in Fig. 4). Further, by incorporating the TOC C^{+--+} detected firstly in this work, the fidelity can reach an impressive 99.9999% (indicated by the blue circles in Fig. 4), which achieves a tenfold enhancement and reaches the requirement of fault-tolerant computing.

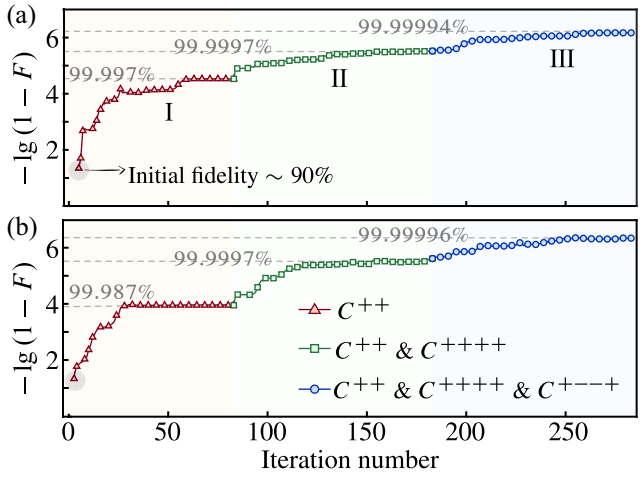

FIG. 4. Quantum optimal control assisted by high-order TOCs. Logarithmic infidelity versus iteration number in the optimization of quantum state transfer sequences for (a) Hadamard gate and (b) Pauli-X gate. The initial states of (a) and (b) are both at $|0\rangle$. The red triangles (stage I), green squares (stage II), and blue circles (stage III) represent the optimization process with the master equation including C^{++}, (C^{++} & C^{++++}), and (C^{++} and C^{++++} and C^{+--+}), respectively. The initial value of each optimization stage is set as the final value of the previous stage.

Discussion and outlook.—We have proposed and demonstrated a protocol for selectively extracting dynamics-complete time-ordered correlations. In comparison with the previous techniques [18–23], our method provides access to an exponentially enlarged set of correlations and is feasible for a wide range of quantum sensors. In the future, the signal-to-noise ratio and spectral resolution of the measured correlations can be further improved by mitigating the decoherence effect [32] and utilizing quantum resources like entanglement and squeezing [33].

Our protocol has potential applications in the fields of quantum information and quantum many-body physics. In one aspect, complete access to TOCs of a quantum bath provides a method to completely characterize quantum noise [31,34,35], which is important to quantum optimal control [36,37]. In another aspect, various TOCs have applications in the characterization of nonequilibrium quantum many-body states [38,39] and dynamics [40–44]. In addition, the effective measurement of TOCs can also be applied to the quantum sensing free of classical noise [24] and the characterization of Bell nonlocality [45], as well as the loophole-free test of macroscopic realism [46].

This work is supported by the Innovation Program for Quantum Science and Technology (Grant No. 2021ZD0303205), National Natural Science Foundation of China (Grants No. 12261160569, No. 12150014, and No. 11927811), Anhui Initiative in Quantum Information Technologies (Grant No. AHY050000), XPLORER Prize, Talents Introduction Foundation of Beijing Normal University (Grant No. 310432106), Guangdong Provincial Quantum Science Strategic Initiative GDZX2200001, the National Key Research and Development Program of China (Project No. 2023ZD0300600), the National Natural Science Foundation of China/Hong Kong RGC Collaborative Research Scheme (Project No. CRS CUHK401/22), and New Cornerstone Science Foundation.

*These authors contributed equally to this work.
†xhpeng@ustc.edu.cn
‡rbliu@cuhk.edu.hk

[1] V. Giovannetti, S. Lloyd, and L. Maccone, Phys. Rev. Lett. **96**, 010401 (2006).

[2] C. L. Degen, F. Reinhard, and P. Cappellaro, Rev. Mod. Phys. **89**, 035002 (2017).
[3] L. Pezzè, A. Smerzi, M. K. Oberthaler, R. Schmied, and P. Treutlein, Rev. Mod. Phys. **90**, 035005 (2018).
[4] G. Brida, M. Genovese, and I. R. Berchera, Nat. Photonics **4**, 227 (2010).
[5] V. Giovannetti, S. Lloyd, and L. Maccone, Nat. Photonics **5**, 222 (2011).
[6] M. Napolitano, M. Koschorreck, B. Dubost, N. Behbood, R. J. Sewell, and M. W. Mitchell, Nature (London) **471**, 486 (2011).
[7] R. Demkowicz-Dobrzanski, J. Kolodynski, and M. Guta, Nat. Commun. **3**, 1063 (2012).
[8] A. Y. Kitaev, arXiv:quant-ph/9511026.
[9] D. Aharonov, J. Cotler, and X. L. Qi, Nat. Commun. **13**, 887 (2022).
[10] B. B. Wei and R. B. Liu, Phys. Rev. Lett. **109**, 185701 (2012).
[11] X. Peng, H. Zhou, B. B. Wei, J. Cui, J. Du, and R. B. Liu, Phys. Rev. Lett. **114**, 010601 (2015).
[12] K. E. Dorfman, F. Schlawin, and S. Mukamel, Rev. Mod. Phys. **88**, 045008 (2016).
[13] G. Gasbarri and L. Ferialdi, Phys. Rev. A **98**, 042111 (2018).
[14] F. M. Haehl, R. Loganayagam, P. Narayan, and M. Rangamani, SciPost Phys. **6**, 001 (2019).
[15] P. Rebentrost, I. Serban, T. Schulte-Herbruggen, and F. K. Wilhelm, Phys. Rev. Lett. **102**, 090401 (2009).
[16] A. Castro and I. V. Tokatly, Phys. Rev. A **84**, 033410 (2011).
[17] B. Hwang and H. S. Goan, Phys. Rev. A **85**, 032321 (2012).
[18] A. Laraoui, F. Dolde, C. Burk, F. Reinhard, J. Wrachtrup, and C. A. Meriles, Nat. Commun. **4**, 1651 (2013).
[19] P. Szankowski, G. Ramon, J. Krzywda, D. Kwiatkowski, and L. Cywinski, J. Phys. Condens. Matter **29**, 333001 (2017).
[20] M. Pfender, P. Wang, H. Sumiya, S. Onoda, W. Yang, D. B. R. Dasari, P. Neumann, X. Y. Pan, J. Isoya, R. B. Liu, and J. Wrachtrup, Nat. Commun. **10**, 594 (2019).
[21] Y. X. Wang and A. A. Clerk, Nat. Commun. **12**, 6528 (2021).
[22] P. Wang, C. Chen, X. Peng, J. Wrachtrup, and R. B. Liu, Phys. Rev. Lett. **123**, 050603 (2019).
[23] J. Meinel, V. Vorobyov, P. Wang, B. Yavkin, M. Pfender, H. Sumiya, S. Onoda, J. Isoya, R. B. Liu, and J. Wrachtrup, Nat. Commun. **13**, 5318 (2022).
[24] Y. Shen, P. Wang, C. T. Cheung, J. Wrachtrup, R. B. Liu, and S. Yang, Phys. Rev. Lett. **130**, 070802 (2023).
[25] A. Cuevas, M. Proietti, M. A. Ciampini, S. Duranti, P. Mataloni, M. F. Sacchi, and C. Macchiavello, Phys. Rev. Lett. **119**, 100502 (2017).
[26] H. Lu, C. Liu, D. S. Wang, L. K. Chen, Z. D. Li, X. C. Yao, L. Li, N. L. Liu, C. Z. Peng, B. C. Sanders, Y. A. Chen, and J. W. Pan, Phys. Rev. A **95**, 042310 (2017).
[27] T. Xin, S. J. Wei, J. S. Pedernales, E. Solano, and G. L. Long, Phys. Rev. A **96**, 062303 (2017).
[28] See Supplemental Material at http://link.aps.org/supplemental/10.1103/PhysRevLett.132.200802 for theoretical aspects of our method, analyses of major experimental error sources and their contributions, some numerical results, as well as additional experimental data and details. These components provide further context and essential information for a more comprehensive understanding of our research, which includes Refs. [29,30].
[29] S. Michaeli, D. J. Sorce, and M. Garwood, Curr. Anal. Chem. **4**, 8 (2008).
[30] M. A. Smith, H. Hu, and A. J. Shaka, J. Magn. Reson. **151**, 269 (2001).
[31] P. Wang, C. Chen, and R. B. Liu, Chin. Phys. Lett. **38**, 010301 (2021).
[32] M. Lassen, M. Sabuncu, A. Huck, J. Niset, G. Leuchs, N. J. Cerf, and U. L. Andersen, Nat. Photonics **4**, 700 (2010).
[33] M. Lassen, L. S. Madsen, M. Sabuncu, R. Filip, and U. L. Andersen, Phys. Rev. A **82**, 021801(R) (2010).
[34] L. M. Norris, G. A. Paz-Silva, and L. Viola, Phys. Rev. Lett. **116**, 150503 (2016).
[35] Y. Sung, F. Beaudoin, L. M. Norris, F. Yan, D. K. Kim, J. Y. Qiu, U. von Lupke, J. L. Yoder, T. P. Orlando, S. Gustavsson, L. Viola, and W. D. Oliver, Nat. Commun. **10**, 3715 (2019).
[36] M. Grace, C. Brif, H. Rabitz, I. A. Walmsley, R. L. Kosut, and D. A. Lidar, J. Phys. B **40**, S103 (2007).
[37] G. Gordon, G. Kurizki, and D. A. Lidar, Phys. Rev. Lett. **101**, 010403 (2008).
[38] T. Schweigler, V. Kasper, S. Erne, I. Mazets, B. Rauer, F. Cataldini, T. Langen, T. Gasenzer, J. Berges, and J. Schmiedmayer, Nature (London) **545**, 323 (2017).
[39] T. Schweigler, M. Gluza, M. Tajik, S. Sotiriadis, F. Cataldini, S. C. Ji, F. S. Moller, J. Sabino, B. Rauer, J. Eisert, and J. Schmiedmayer, Nat. Phys. **17**, 559 (2021).
[40] G. A. Áarez, D. Suter, and R. Kaiser, Science **349**, 846 (2015).
[41] A. M. Kaufman, M. E. Tai, A. Lukin, M. Rispoli, R. Schittko, P. M. Preiss, and M. Greiner, Science **353**, 794 (2016).
[42] R. J. Lewis-Swan, A. Safavi-Naini, A. M. Kaufman, and A. M. Rey, Nat. Rev. Phys. **1**, 627 (2019).
[43] D. A. Abanin, E. Altman, I. Bloch, and M. Serbyn, Rev. Mod. Phys. **91**, 021001 (2019).
[44] J. Randall, C. E. Bradley, F. V. van der Gronden, A. Galicia, M. H. Abobeih, M. Markham, D. J. Twitchen, F. Machado, N. Y. Yao, and T. H. Taminiau, Science **374**, 1474 (2021).
[45] N. Brunner, D. Cavalcanti, S. Pironio, V. Scarani, and S. Wehner, Rev. Mod. Phys. **86**, 419 (2014).
[46] P. Wang, C. Chen, H. Liao, V. V. Vorobyov, J. Wrachtrup, and R.-B. Liu, arXiv:2401.05246.